Chip-Scale Room-Temperature Atomic Magnetometers for Biomedical Measurements

S. Knappe[1,2], R. Mhaskar[1,2], J. Preusser[1], J. Kitching[1], L. Trahms[3], and T. Sander[3]

[1] Time and Frequency Division, NIST, Boulder CO, USA
[2] University of Colorado, Boulder CO, USA
[3] Physiklisch-Technische Bundesanstalt, Berlin, Germany

Abstract— **We describe a portable four-channel array of chip-scale atomic magnetometers in a flexible flying-lead configuration. These microfabricated, uncooled sensors with volumes below 1 cm^3 demonstrate sensitivities around 100 fT/Hz$^{1/2}$ and bandwidths of several hundred hertz. Performance limits are discussed, as the design is easily scalable to different sensor sizes and large arrays. Initial measurements of MCG are cross-validated with SQUID measurements.**

Keywords— **Chip-scale atomic magnetometer, MCG, MEG, MRX, optical magnetometer**

I. Introduction

In clinical as well as applied research laboratory settings, the best measurements of biomagnetic signals from the human heart and brain are still performed with superconducting quantum interference devices (SQUIDs). With sensitivities of a few femtotesla/Hz$^{1/2}$ over a large frequency range, SQUIDs allow for the most sensitive measurements of the body's magnetic fields. Recently, however, several room-temperature magnetic sensors are being developed that could be used for the less demanding measurements of biomagnetism. Among those are magnetoresistive devices [1], multiferroics [2, 3], and atomic magnetometers [4]. Atomic or optical magnetometers with sensitivities below 1 fT/Hz$^{1/2}$ [5] have been demonstrated in laboratory prototypes, and initial measurements of magnetocardiography (MCG) [6] and magnetoencephalography (MEG) [7] have been recorded. Despite these initial demonstrations, many advances are still required before atomic magnetometers fully compete with SQUID arrays [8], but their success would allow for less-expensive, easy-to-use systems that might enable a more widespread use of biomagnetism in biomedical applications.

II. Chip-Scale Atomic Magnetometers (CSAMs)

A microfabricated version of atomic magnetometers is particularly attractive, because fabrication methods lent from microelectromechanical (MEMS) systems can allow for parallel fabrication of large sensor arrays with tight tolerances. These methods enable relatively easy scaling of such devices from sizes of several micrometers to several millimeters. The fundamental sensitivity of atomic magnetometers limited by the shot noise of the atoms and photons has been predicted to be just below 1 fT/Hz$^{1/2}$ for a 1 mm^3 volume filled with a gas of ^{87}Rb atoms [9, 10]. Figure 1 (left, blue) shows this sensitivity as a function of cell size. The sensitivity of atomic magnetometers is predicted to be flat over a large frequency range limited on the low side by slow drifts and on the high side by the bandwidth of the magnetometer. The bandwidth associated with this fundamental sensitivity is also shown in Figure 1 (right, red), given by the resonance width. It is worth mentioning that larger bandwidth can always be achieved by trading off some sensitivity. Nevertheless, the fundamental sensitivity limit has not been reached experimentally in these atomic vapors. The best sensitivity in a 1 mm^3 volume demonstrated to date is 5 fT/Hz$^{1/2}$ [11], a factor of seven worse than the fundamental value, and is suspected to be limited by magnetic noise from parts of the sensor itself and the vicinity of the sensor.

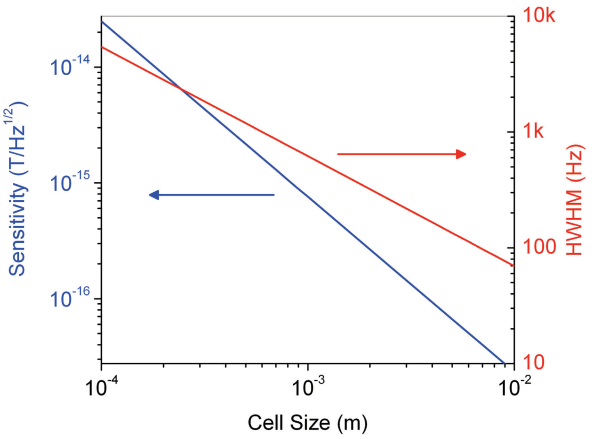

Fig. 1 Fundamental sensitivity and bandwidth (given by the HWHM of the resonance) of a ^{87}Rb atomic magnetometer as a function of size, when limited by photon and atom shot noise

To operate these CSAMs, a vapor of ^{87}Rb atoms is optically pumped by laser light, resonant with an optical transition ($5S_{1/2} \rightarrow 5P_{1/2}$) of the atoms. An ambient gas of nitrogen broadens this optical transition to 20 GHz so that the hyperfine structure is not resolved. The light is circularly polarized and transfers angular momentum from the photons to the

Á. Jobbágy (Ed.): 5th European IFMBE Conference, IFMBE Proceedings 37, pp. 1330–1333, 2011.
www.springerlink.com

atoms, so that the atoms become spin-polarized. This macroscopic magnetization of the gas precesses in an ambient magnetic field at a well-defined Larmor frequency of roughly 7 Hz/nT. The orientation of the atomic spins can be monitored through the absorption or dispersion of a near-resonant light beam, which is used to read out the magnetic field value. A schematic of the magnetometer setup and its principle of operation is shown in Figure 2. The pump laser creates a spin-polarization in the Rb atoms along z, and a perpendicular probe laser monitors the rotation of the spins into the direction x, which is proportional to the component of the magnetic field along y. This type of atomic magnetometer is therefore a directional sensor sensitive to magnetic fields parallel to y.

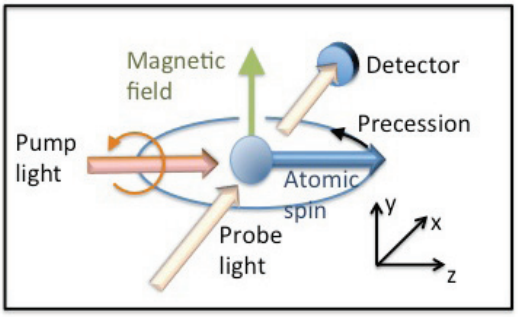

Fig. 2 Principle of operation for a directional atomic magnetometer sensitive to a magnetic field in the y direction. The pump light orients the atomic spins. They precess in a magnetic field at a well-defined frequency. A probe laser detects the rotation of the spins into x-direction.

In order to reach sensitivities close to the ones quoted in Figure 1, the magnetometer has to be operated in a regime where a loss of coherent spin precession due to spin-exchange collisions between the Rb atoms is suppressed [12]. This can be achieved with high atomic densities in low magnetic fields [13]. Therefore, the dynamic range of these magnetometers is limited to roughly 100 nT.

A simplified version of such magnetometers can be operated with just one laser beam, which can simultaneously act as a pump and probe laser [9]. An oscillating magnetic field deliberately applied to the atoms perpendicular to the laser beam then defines the sensitive direction of the magnetometer when the transmission of the light though the cell at the oscillation frequency is monitored. When two fields are applied at different frequencies, magnetic fields in the directions x and y can be monitored simultaneously.

The picture of such a chip-scale atomic magnetometer is shown in Figure 3. The laser and photodetectors are housed inside a control box and the light is transmitted to the sensor heads that contain the Rb vapor through optical fibers, as shown in the schematic on the left side of Figure 3. This allows for magnetic components such as the laser to be placed several meters away from the sensor heads, and allows a single laser to power a whole array of sensor heads.

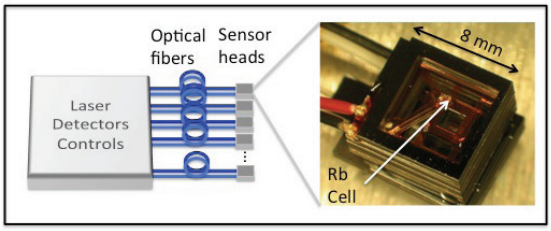

Fig. 3 Left: Schematic of the chip-scale atomic magnetometer array. Optical fibers connect the sensor heads with a control system in a flexible geometry. Right: Photograph of a CSAM sensor head that houses the vapor cell on a polyimide web.

The photograph on the right in Figure 3 shows a MEMS sensor head that contains the vapor cell [14] with heaters on both windows to choose the Rb vapor pressure, suspended on a polyimide webbing to reduce thermal losses [15]. Thin-film heaters are deposited onto glass substrates that sit on both windows of the vapor cell. They raise the Rb vapor pressure inside the cell and therefore set the number of atoms in the vapor that can be polarized. In order not to disturb the magnetic field measurements with currents flowing through the heaters, an alternating current at 30 kHz is used to drive the heaters. This frequency is well outside the bandwidth of the chip-scale magnetometers. Micro-optical components direct the light between the input and output fiber through the vapor cell. They consist of micro-prisms for beam steering, polarizers and quarter-wave plates to define the circular polarization, and lenses to collimate the beam through the cell and focus it back into the fiber.

Initial biomagnetic measurements recorded with these chip-scale magnetometers include MCGs [16], magnetorelaxometry (MRX) of nanoparticles [16], and MEGs of healthy human subjects. They have been performed inside a magnetically shielded room BMSR-2 [17] at the Physikalisch-Technische Bundesanstalt (PTB) in Berlin. The measurements have been validated with data taken with a multi-channel low-temperature SQUID system [18]. All typical features were resolved in both the CSAM data and the simultaneously taken SQUID data. Part of the higher noise level of a CSAM magnetocardiogram with respect to SQUID based MCG can be compensated by the higher signal that is due to the shorter distance of the CSAM from the skin. The

sensitivity of the CSAM sensors was measured to be 100 to 200 fT/Hz$^{1/2}$ with a bandwidth of several hundred hertz.

Furthermore, MCG maps were measured with a single sensor that was sequentially scanned over an area of the chest of healthy volunteers at a distance of 1 cm. Interpolated field maps of the normal component of the magnetic field are shown in Figure 4 for one volunteer. The green markers in the CSAM time traces on the top show the temporal position of the maps. Since unaveraged sequentially measured data were used, the time traces measured at each scan position had to be baseline corrected by subtracting the average value in the baseline window indicated in red of the trace. The scan area represented in the maps is centered at a position 5 cm to the left of the sternum and 6 cm below the jugulum. The contour step size is 4.5 pT and the black dots in the right map represent the sensor positions during the scan.

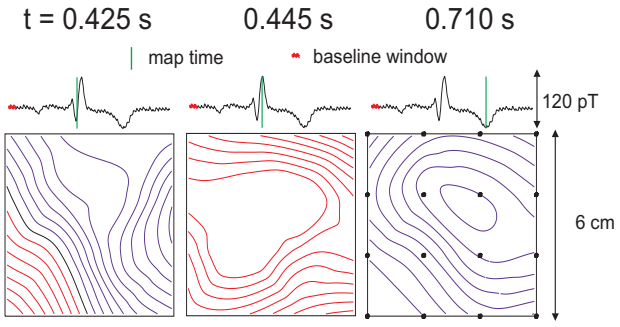

Fig. 4 Maps of the normal component of the magnetic field of the human heart measured at approximately 1 cm over the chest. Data were sequentially detected with one CSAM. The three maps represent three different times during the heart cycle, corresponding to the green lines in the traces above the maps. The traces are unaveraged data measured with the CSAM. Center of maps: 5 cm left of the sternum and 6 cm below the jugulum. Contour steps: 4.5 pT. Blue: positive values, red: negative values with respect to the baseline. Black dot in right map represent the 16 sensor positions covered by the scan.

In comparison to the SQUID based MCG recordings, the amplitudes of the CSAM are more than two times higher. This improvement of the signal amplitude is owed to the smaller distance between sensor and source.

While only a small CSAM sensor array of four sensors was tested, we predict that up to 100 sensors can be powered by the same laser. Finally, with similar sensors, sensitivities below 20 fT/Hz$^{1/2}$ have been measured in a laboratory environment.

III. CONCLUSIONS

We have demonstrated a four-channel array of chip-scale atomic magnetometers in a flying-lead configuration. They potentially present an inexpensive thermally much easier to handle alternative to SQUID magnetometers that allows for flexible geometries of large sensor arrays for less demanding biomedical applications. While initial demonstrations of their capabilities in biomedical measurements such as MCG, MEG, and MRX look promising, further validation and improvements are planned.

ACKNOWLEDGMENT

We thank S. Schima for fabrication of the magnetometer components. This work is a contribution of NIST, an agency of the US government, and is not subject to copyright.

REFERENCES

1. Chaves RC, Freitas PP, Ocker B et al. (2007) Low frequency picotesla field detection using hybrid MgO based tunnel sensors. Appl Phys Lett 91: 102504
2. Cheong S-W, Mostovoy M (2007) Multiferroics: a magnetic twist for ferroelectricity. Nat Mater 6: 13-20
3. Dong S, Li J-F, Viehland D (2003) Ultrahigh magnetic field sensitivity in laminates of TERFENOL-D and Pb($Mg_{1/3}Nb_{2/3}$)O_3--$PbTiO_3$ crystals. Appl Phys Lett 83: 2265-2267
4. Budker D, Romalis M (2007) Optical magnetometry. Nat Phys 3: 227-234
5. Dang HB, Maloof AC, Romalis MV (2010) Ultrahigh sensitivity magnetic field and magnetization measurements with an atomic magnetometer. Appl Phys Lett 97: 151110
6. Bison G, Castagna N, Hofer A et al. (2009) A room temperature 19-channel magnetic field mapping device for cardiac signals. Appl Phys Lett 95: 173701
7. Xia H, Baranga AB-A, Hoffman D et al. (2006) Magnetoencephalography with an atomic magnetometer. Appl Phys Lett 89: 211104-211103
8. Wikswo JPJ (2004) SQUIDs remain best tools for measuring brain's magnetic fields. Phys Today 57: 15-17
9. Shah V, Knappe S, Schwindt PDD et al. (2007) Subpicotesla atomic magnetometry with a microfabricated vapour cell Nature Photonics 1: 649-652
10. Ledbetter MP, Savukov IM, Acosta VM et al. (2008) Spin-exchange-relaxation-free magnetometry with Cs vapor. Phys Rev A 77: 033408
11. Griffith WC, Knappe S, Kitching J (2010) Femtotesla atomic magnetometry in a microfabricated vapor cell. Opt Express 18: 27167-27172
12. Allred JC, Lyman RN, Kornack TW et al. (2002) High-sensitivity atomic magnetometer unaffected by spin-exchange relaxation. Phys Rev Lett 89: 130801
13. Happer W, Tang H (1973) Spin-Exchange Shift and Narrowing of Magnetic Resonance Lines in Optically Pumped Alkali Vapors. Phys Rev Lett 31: 273
14. Liew LA, Knappe S, Moreland J et al. (2004) Microfabricated alkali atom vapor cells. Appl Phys Lett 84: 2694-2696

15. Mescher MJ, Lutwak R, Varghese M (2005) An ultra-low-power physics package for a chip-scale atomic clock. IEEE Solid-State Sensors and Actuators pp. 311-316.
16. Knappe S, Sander TH, Kosch O et al. (2010) Cross-validation of microfabricated atomic magnetometers with superconducting quantum interference devices for biomagnetic applications. Appl Phys Lett 97: 133703
17. Bork J, Hahlbohm HD, Klein R et al. (2001) The 8-layered magnetically shielded room of the PTB: Design and construction. Proc 12th Int Conf on Biomagnetism, pp. 970-973.
18. Schnabel A, Burghoff M, Hartwig S et al. (2004) A sensor configuration for a 304 SQUID vector magnetometer. Neurology clinical neurophysiology 2004: 70